

Ultra-hard carbon film from epitaxial two-layer graphene

Yang Gao^{1,2}, Tengfei Cao^{1,3}, Filippo Cellini¹, Claire Berger^{2,4}, Walter A. de Heer², Erio Tosatti^{5,6},
Elisa Riedo^{1,2,7,8*} and Angelo Bongiorno^{3,8,9*}

Atomically thin graphene exhibits fascinating mechanical properties, although its hardness and transverse stiffness are inferior to those of diamond. So far, there has been no practical demonstration of the transformation of multilayer graphene into diamond-like ultra-hard structures. Here we show that at room temperature and after nano-indentation, two-layer graphene on SiC(0001) exhibits a transverse stiffness and hardness comparable to diamond, is resistant to perforation with a diamond indenter and shows a reversible drop in electrical conductivity upon indentation. Density functional theory calculations suggest that, upon compression, the two-layer graphene film transforms into a diamond-like film, producing both elastic deformations and sp^2 to sp^3 chemical changes. Experiments and calculations show that this reversible phase change is not observed for a single buffer layer on SiC or graphene films thicker than three to five layers. Indeed, calculations show that whereas in two-layer graphene layer-stacking configuration controls the conformation of the diamond-like film, in a multilayer film it hinders the phase transformation.

Carbon can form different types of materials, from diamond to graphite and more recently fullerenes, nanotubes and graphene, which exhibit a variety of exceptional properties. Sintering materials with a stiffness and hardness equal or superior to those of diamond is an ongoing challenge^{1–3}. Thus, for both scientific and technological reasons, the transformation of graphite into diamond remains one of the most fascinating and studied solid-to-solid phase transitions in materials science^{2,4–12}. Recently, experimental^{13–16} and theoretical^{10,17,18} efforts have been directed at studying the transformation of multilayer graphene into a diamond-like structure, induced by chemical functionalization of the surface layers. Unfortunately, despite recent successes^{13,14}, the experimental proof that such atomically thin diamond-like films exhibit mechanical properties similar to those of diamond remains missing.

Here, we use sub-ångström-resolution modulated nano-indentation (MoNI)¹⁹ atomic force microscopy (AFM) experiments, microhardness and conductive AFM measurements and density functional theory (DFT) calculations to investigate the mechanical properties of multilayer graphene films on SiC. Our study shows that, at room temperature, indentation in a two-layer (2-L) epitaxial graphene film grown on SiC(0001) induces a reversible transformation from a graphitic to a diamond-like structure, resulting in stiffness and hardness values comparable to those of diamond. In particular, in our MoNI experiments¹⁹, a Si spherical probe with a radius of 120 nm is used to indent SiC and epitaxial graphene films of various thicknesses, reaching loads on the order of 100 nN, corresponding to pressures of ~1–10 GPa considering the contact area between the spherical tip and the flat substrate and indentation depths ranging from 0.6 to 6 Å, depending on the thickness of the multilayer graphene film. After indenting a multilayer graphene film on SiC, force versus indentation curves were collected while retracting the tip with sub-ångström resolution. These experiments

show that the transverse elastic modulus of multilayer graphene on SiC(0001) with number of layers larger than five is close to the Young's modulus of graphite in the direction perpendicular to the basal plane, that is, ~30 GPa, whereas for a single carbon layer on SiC(0001)—the graphene buffer layer—Young's modulus is the same as that of a bare SiC substrate. Surprisingly, our MoNI measurements show that the transverse stiffness of 2-L epitaxial graphene on SiC(0001) is much larger than that of the bare substrate, that is, >400 GPa. Furthermore, microhardness measurements show that 2-L epitaxial graphene resists plastic deformations upon indentation with a diamond indenter, even at maximum loads of 30 μ N, whereas similar loads can easily produce holes in both SiC and multilayer epitaxial graphene for films thicker than 5-L. DFT calculations indicate that the unique mechanical response to indentation of 2-L graphene stems from its ability to undergo a structural transformation into a diamond-like film and that this ability is hindered in 3-L or thicker films by unfavourable layer-stacking configurations. This theory is further confirmed by the experimental observation of a reversible decrease in electrical conductivity induced by indentation in 2-L graphene, which is absent in 5-L graphene. In particular, our DFT calculations show that the sp^2 to sp^3 structural changes in a 2-L graphene film on SiC(0001) are facilitated by the presence of a buckled buffer layer in contact with the incommensurable and reactive Si-terminated face of the SiC substrate, that they occur upon indentation regardless of the nature of the layer-stacking configuration and that the resulting diamond-like film does not necessitate the presence of adsorbates to passivate and stabilize the surface of the film in contact with the indenter.

Stiffness experiments

Graphene films were grown epitaxially on the SiC(0001) surface by thermal sublimation^{20,21}. Sub-ångström-resolved nano-indentation

¹Advanced Science Research Center, City University of New York, New York, NY, USA. ²School of Physics, Georgia Institute of Technology, Atlanta, GA, USA. ³Department of Chemistry, College of Staten Island, City University of New York, Staten Island, NY, USA. ⁴Institut Néel, CNRS- University Grenoble-Alpes, Grenoble, France. ⁵Abdus Salam ICTP, Trieste, Italy. ⁶SISSA, Trieste, Italy. ⁷Physics Department, City College of New York, City University of New York, New York, NY, USA. ⁸CUNY Graduate Center, Ph.D. Program in Physics, New York, NY, USA. ⁹CUNY Graduate Center, Ph.D. Program in Chemistry, New York, NY, USA. Yang Gao and Tengfei Cao contributed equally to this work. *e-mail: elisa.riedo@asrc.cuny.edu; angelo.bongiorno@csi.cuny.edu

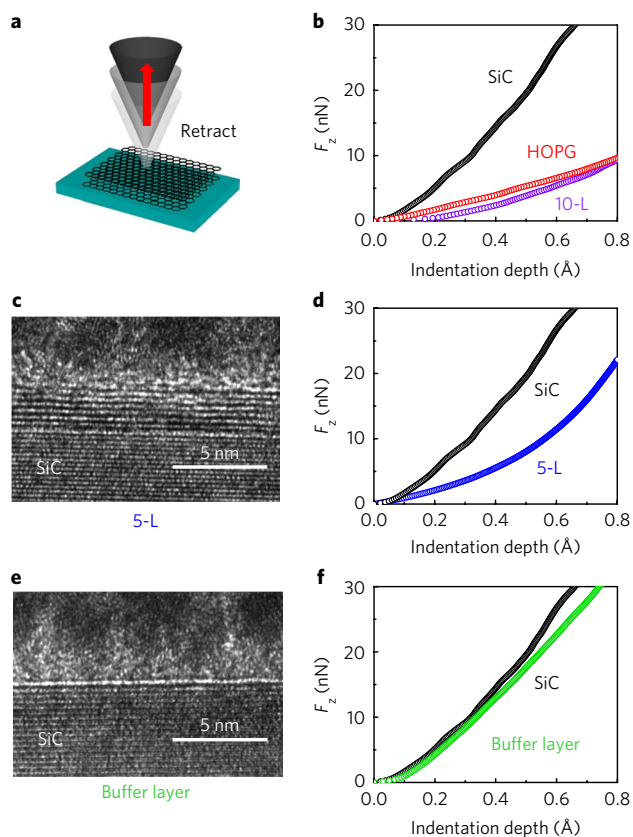


Fig. 1 | TEM images and experimental stiffness curves for multilayer epitaxial graphene and buffer layer on SiC. **a**, Schematics of the experiments performed in retracting mode. **b**, Indentation curves of SiC, HOPG and 10-L graphene on SiC (000–1). **c,d**, TEM image (**c**) and indentation curve (**d**) of 5-L graphene on SiC (0001). **e,f**, TEM image (**e**) and indentation curve (**f**) of the buffer layer on SiC(0001). The MoNI curves in **b**, **d** and **f** are taken with the same tip and are averaged over 10 curves (Supplementary Figs. 4 and 5). Experimental errors are $\Delta F_z = 0.5$ nN and $\Delta z = 0.01$ nm. Scale bars (**c,e**), 5 nm.

curves were obtained by MoNI (for more details see Methods section and Supplementary Information Section 1)¹⁹. In the MoNI experiments, a silicon tip is brought into hard contact with a graphene film. The tip indents the sample until it reaches a normal force of 50–300 nN. The actual measurement is taken after forming the hard contact, that is, during the process of retracting the AFM tip from the supported film at a rate of ~ 0.01 nm s⁻¹ (Fig. 1a). At this point the normal force is gradually reduced while the tip holder is oscillated vertically with an amplitude of ~ 0.1 Å, at a fixed frequency, by means of a lock-in amplifier. For each value of the normal force between tip and sample, F_z (which is controlled and kept constant by the feedback loop of the AFM), a lock-in amplifier is used to measure the slope of the force versus indentation depth curve, namely the contact stiffness $k_{\text{cont}}(F_z)$ (ref. 19). Force versus indentation depth curves with sub-ångström resolution are then obtained by integrating the equation $dF_z = k_{\text{cont}}(F_z) dz_{\text{indent}}$ as follows:

$$z_{\text{indent}}(F_z) = \int \frac{dF_z'}{k_{\text{cont}}(F_z')} \quad (1)$$

For simplicity, and despite its limitations, we use the Hertz model to extract elastic moduli from our experimental force versus indentation

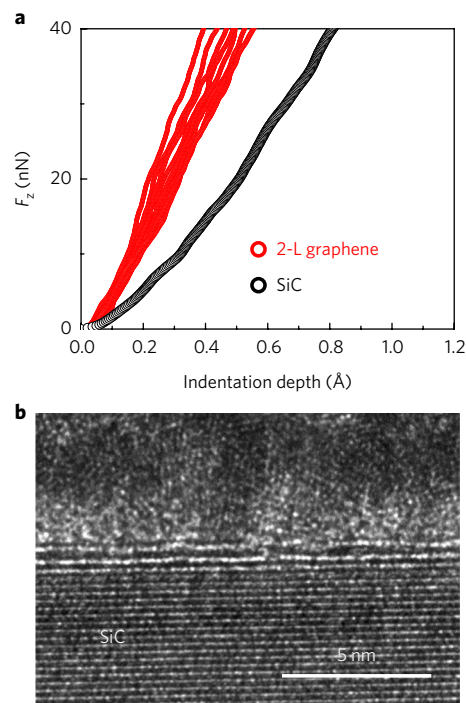


Fig. 2 | Experimental stiffness measurements in 2-L graphene.

Experiments show a new ultrastiff phase in 2-L graphene at room temperature upon indentation. **a**, Experimental indentation curves in 2-L epitaxial graphene (red) and SiC (black). For 2-L graphene, curves were acquired at different positions on different samples. **b**, TEM image of 2-L epitaxial graphene on SiC. Scale bar, 5 nm.

depth curves. In previous studies, MoNI measurements and the Hertz model were used successfully to probe and characterize the elasticity of bulk materials, including very stiff materials such as SiC (Fig. 1b), as well as the radial elasticity of nanotubes and the interlayer elasticity in graphene oxide films^{19,22–24}. We underline the fact that the high resolution of the indentation curves obtained from MoNI experiments allows measurement of the Young's modulus of materials stiffer than the Si tip.

We used the MoNI technique to probe the vertical elastic moduli of 10-L, 5-L, 2-L and single-layer graphene in contact with the Si-face of SiC(0001), that is, the buffer layer. In these experiments, the maximum indentation depth ranged from 0.6 Å in the case of 2-L graphene up to 6 Å for 10-L graphene, and the experimental errors for the tip normal force F_z and indentation depth were $\Delta F_z = 0.5$ nN and $\Delta z = 0.01$ nm, respectively. To probe the number of layers in the graphene films, we performed transmission electron microscopy (TEM) and scanning TEM (STEM) measurements, as well as Raman spectroscopy and Kelvin probe force microscopy (KPFM) experiments. TEM images and force versus indentation depth curves of 5-L graphene, the buffer layer and 2-L graphene are shown side by side in Figs. 1 and 2 (see Supplementary Information). The indentation curves in Fig. 1 were obtained by averaging more than ten curves obtained from MoNI measurements of different spots on different samples. In Fig. 1b, the indentation curve of 10-L graphene²⁵ is very close to that obtained for bulk highly ordered pyrolytic graphite (HOPG)¹⁹. The elastic modulus derived by fitting the indentation curve for 10-L graphene with a Hertz model is ~ 36 GPa, very close to the *c*-axis Young's modulus of graphite^{19,26} (the indentation curve for 10-L reaching a depth of 6 Å is reported in Supplementary Fig. 5). Figure 1d,f shows the indentation curves of a bare SiC substrate together with the curves of a supported 5-L

graphene film and the buffer layer, respectively. Analysis of the indentation curve of SiC yields, in agreement with published values¹⁹, a Young's modulus of 400 GPa, whereas the curves for the buffer layer and the 5-L film clearly show that coating SiC with a graphene film leads to a softening of the elastic modulus measured by the MoNI technique. Although the exact nature of the buffer layer is still under scrutiny²¹, the notion that it consists of a graphene layer strongly interacting with the SiC substrate is well accepted, so it is not surprising that its effect on the indentation curve is detectable, but mild. On the other hand, a 5-L graphene film exhibits a transverse elastic modulus comparable to that of a graphitic system^{19,26} and its softening effect on the elastic modulus of the entire system (substrate plus 5-L film) is significant and almost comparable to that of a 10-L graphene film. Overall, all these elastic behaviours are expected and well understood to arise when a rigid substrate is coated by a thin film of a softer material of increasing thickness, and indeed the indentation curves for 10-L, 5-L and buffer-layer graphene on SiC follow a predictable trend. However, and very surprisingly, when we indent two layers of graphene on SiC, as shown in Fig. 2a (and the corresponding TEM image in Fig. 2b), we obtain force versus indentation curves that are much steeper than those for 5-L or 10-L graphene and even steeper than bare SiC. Such large stiffness for 2-L epitaxial graphene corresponds to a transverse Young's modulus much larger than the modulus of SiC, that is, $\gg 400$ GPa, indicating that a 2-L graphene film can significantly enhance the stiffness of the substrate. The Hertz model is appropriate for isotropic bulk materials, so a simple Hertz fit is inadequate here to extract from these elastic indentation curves the exact value of the transverse Young's modulus of the isolated atomically thin 2-L film. Nevertheless, the experimental elastic indentation curves of 2-L graphene on SiC clearly indicate that important physical/chemical effects must happen in the 2-L film to explain the stiffening effect produced by coating SiC(0001) with a 2-L graphene film. Our computational modelling work (vide infra), in agreement with recent theoretical works^{17,18} and indentation studies of suspended single-layer graphene²⁷, suggests that the ultrastiffening caused by 2-L graphene is due to a transformation from a layered into a diamond-like structure occurring in the 2-L carbon film upon indentation, namely when the AFM tip approaches and presses upon the supported film.

Microhardness and C-AFM upon indentation

To further challenge the existence of a diamond phase induced by pressure in 2-L epitaxial graphene, we perform microhardness experiments (Fig. 3a–d) with a diamond indenter using loads up to 12 μ N on 2-L and 5-L graphene films on SiC(0001), as well as on a bare SiC substrate (for more details and measurements see Methods and Supplementary Fig. 6). Quite unexpectedly, although in agreement with our MoNI measurements, upon indentation and after subsequent AFM topographic imaging, no residual indent is found in 2-L epitaxial graphene on SiC (Fig. 3a), indicating a hardness value close if not superior to that of the diamond indenter. By contrast, when indenting a bare SiC sample with the same indenter and load, we were able to identify a residual indent (diameter of ~ 30 – 40 nm; Fig. 3b). Furthermore, a larger and deeper residual indent is observed when indenting, with the same conditions, 5-L epitaxial graphene (diameter ~ 60 – 70 nm), as shown in Fig. 3c. For completeness, we note that these experiments led us to estimate a hardness^{28,29} for SiC of 20 ± 10 GPa (see Methods for details), which is close to hardness values reported in the literature^{30,31}, as well as a value of hardness for the 5-L graphene film on the order of 5 ± 2 GPa, which is similar to the hardness of HOPG²⁸.

To further investigate the pressure-activated carbon phase, we carried out load-dependent conductive AFM (C-AFM) experiments on 2-L and 5-L graphene films on SiC (Fig. 3e). These experiments were conducted by using a metallic AFM tip to apply pressure

and simultaneously collect the electrical current flowing between the tip and a silver electrode deposited on the graphene film surface under the influence of a constant voltage bias (Supplementary Fig. 7). Current measurements were taken while varying the tip load from 200 to 400 nN. Figure 3e displays the current measurements for 5-L and 2-L graphene films on SiC. In the 5-L film, the current increases with increasing normal load, consistent with the increase in contact area and hence the electrical contact between tip and film. By contrast, for 2-L films these experiments show that although the current initially increases with load, for loads >260 nN the current suddenly drops, suggesting that at these loads the 2-L film undergoes a phase transition to a structure with a larger sp^3 content and thus more resistive. C-AFM experiments on different 2-L samples (for example, the two samples shown in Fig. 3e) but with the same AFM tip show that the structural transition occurs consistently at a critical load of ~ 270 nN. We note that the observed decrease in electrical conductivity induced by indentation in 2-L graphene is fully reversible on decreasing the load, suggesting a spontaneous healing of the transformed nucleus taking place at room temperature. Variations in the observed absolute values of current in the different films are attributable to inhomogeneity of the film surface, the quality of the silver contact, the distance between the measured region and silver electrode, and tunnelling phenomena at the periphery of the tip–film contact.

DFT and indentation simulations

MoNI, microhardness and C-AFM experiments show that the behaviour upon compression of a 2-L graphene film on SiC(0001) is inconsistent with that of a substrate coated by a carbon film with a graphitic-like structure, which should lead to a softening of the transverse elasticity as observed in the case of a 5-L or 10-L film on SiC. Our DFT calculations and classical indentation simulations based on Hookean force fields indicate that the ultrastiffness exhibited by 2-L graphene on SiC arises from a mechano-chemical effect; namely, in addition to deformations, the mechanical load on the supported 2-L graphene film produces sp^2 to sp^3 structural and chemical changes, ultimately leading to the formation of a stiff diamond-like film coating the SiC substrate. Calculations and results of our modelling study are discussed in full in the Supplementary Information.

A graphene film interacts strongly with the Si-face of a SiC(0001) substrate. To gain insight into how this interface may influence elastic properties and structural transformations of a carbon film supported by SiC, we considered model structures of 2-L, 3-L and 4-L graphene films sandwiched between simplistic representations of a SiC(0001) surface, consisting of a single SiC(0001) layer with Si atoms in contact with the bottom and top layers of the carbon films and the C atoms saturated by H atoms. We considered multilayer graphene films with several different layer-stacking configurations, as well as supercells of increasing lateral size, to mimic different interfacial structures and account for the incommensurability of the graphene buffer layer and SiC(0001). For each model structure, we carried out a sequence of DFT optimization calculations, in which the C atoms of the SiC layers are constrained to lie on planes at a fixed separation. These DFT calculations show that 2-L graphene can transform upon compression into a diamond-like film in contact with SiC(0001) (Fig. 4a). The sp^2 to sp^3 structural and chemical changes occur regardless of the stacking configuration of the two graphene layers, are favoured by buckling distortions of the buffer layer in contact with the reactive SiC(0001) substrate, and occur more favourably (that is, the energy cost associated to the homogeneous transformation vanishes) by reducing the lattice mismatch at the interface between the substrate and buffer layer (Supplementary Fig. 12). Moreover, DFT calculations show that the phase transformation to a diamond-like film in compressed 3-L and 4-L graphene films is hindered by the layer-stacking configuration. In particular,

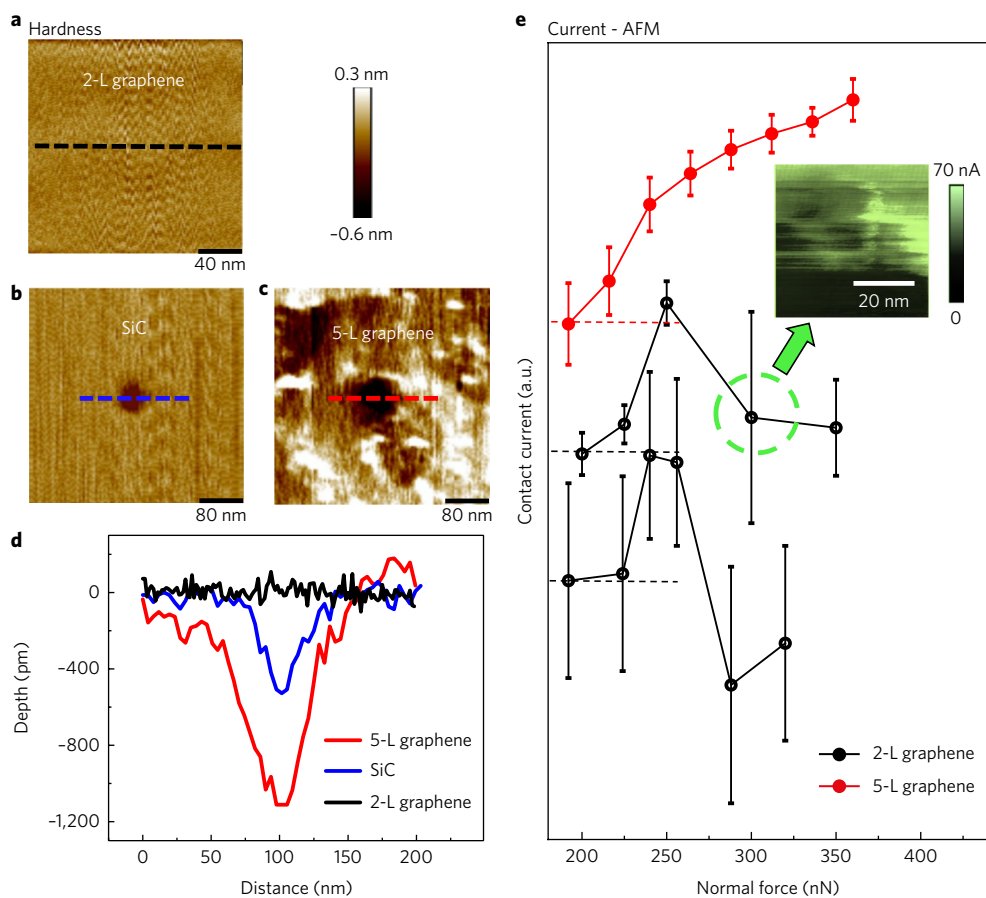


Fig. 3 | Microhardness and C-AFM measurements. **a–c**, AFM topographical images of residual indents in 2-L graphene (**a**), SiC (**b**) and 5-L graphene (**c**) upon indentation with a diamond indenter. **d**, Cross-section profile of residual indents in 2-L graphene, SiC and 5-L graphene, as shown in the AFM topographic images in **a–c**, respectively. **e**, Three stacked curves of the average current signal versus normal load, measured with C-AFM (Supplementary Fig. 7) on $50 \times 50 \text{ nm}^2$ areas on two different 2-L graphene films (black curves) and a 5-L graphene film (red curve). A current drop is observed at $\sim 260 \text{ nN}$ only for 2-L graphene samples. Inset: Current image recorded on 2-L graphene at 300 nN while scanning from top to bottom, indicating a drop in current occurring after a few scans. These current versus load curves are reversible on decreasing the load.

our calculations show that whereas a 3-L or 4-L graphene film with ABC (rhombohedral) or AAA (hexagonal) stacking configuration can transform upon compression into a diamond-like film, a film with the AB (Bernal) stacking configuration typical of multilayer graphene and graphite undertakes only partial sp^2 to sp^3 structural changes (Supplementary Fig. 13). In this latter case, the unfavourable layer stacking prevents the graphitic-to-diamond transition from propagating across the entire transverse direction of the film. DFT calculations based on these types of model structure (Fig. 4a and Supplementary Information) also show that a diamond-like film forms a hard contact with the SiC(0001) substrate, exhibiting an interfacial layer of bonds with a transverse elasticity (or elastic modulus) as stiff as that of the substrate material. This important result is accounted for in our indentation simulations based on atomistic Hookean force fields (vide infra).

We used DFT calculations to investigate the structure, mechanical and electronic properties of diamond-like films resulting from compression of a 2-L graphene film (Supplementary Figs. 8–10). These calculations show that, regardless of the stacking configuration, two graphene layers buckle to form a diamond-like film, exposing dangling bonds towards the vacuum region. Here, we construct six possible configurations for a diamond-like film resulting from compressing a 2-L graphene film with AA, AB or $A_B C$ stacking configuration ($A_B C$ is used here to indicate the stacking configuration resulting when the midpoints between bonded A and B sites of one

layer are aligned along the transverse direction with the C sites of the second layer). In this case, we use H to saturate the dangling bonds exposed by the surfaces of the films (Fig. 4b) and we use DFT calculations to estimate the transverse elastic modulus of the hydrogenated diamond-like films, finding values ranging from 0.30 up to 1.01 TPa, close to the Young's modulus calculated for bulk diamond. The stiffest film has the structure of hexagonal diamond (lonsdaleite³², Supplementary Fig. 9) and it results from compressing two graphene layers stacked in an AA configuration. We also note that two of these six conformations for a diamond-like film exhibit surface geometries showing the occurrence of broken resonance structures. DFT calculations show that the removal of H atoms from one of the two equivalent surfaces of these two diamond-like films leads to energetically stable and insulating carbon films, exhibiting an electronic bandgap of $\sim 2 \text{ eV}$ (Fig. 4c) and exposing a clean and chemically inert surface to the vacuum. These results are in agreement with recent DFT studies^{7,17,18}.

DFT calculations show that, upon compression, a 2-L graphene film on SiC(0001) transforms into a diamond-like film with a Young's modulus of up to 1.01 TPa. The interface between the carbon film and substrate consists of a thin layer of bonds whose transverse mechanical strength is comparable to that of bulk SiC, whereas the surface of the diamond-like film consists of either chemically inert regions exposing for instance the well-known dimer C–C reconstruction (Fig. 4c) or regions with dangling

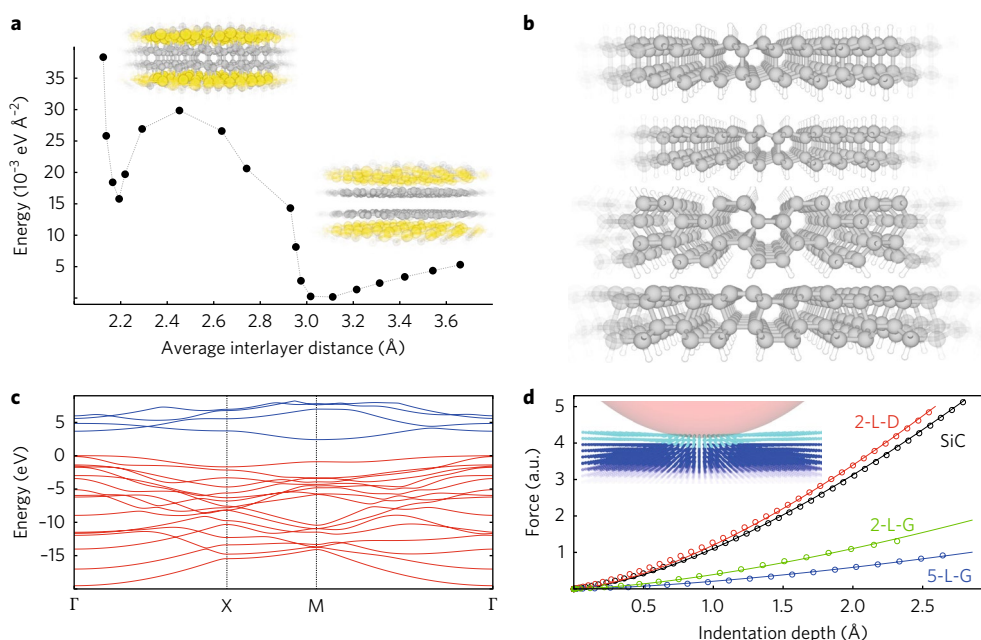


Fig. 4 | DFT and indentation calculations. **a**, Energy per unit area obtained by DFT calculations for a 2-L graphene film sandwiched between mirroring H-CSi layers. The graphene layers include 4×4 elementary unit cells in contact with a SiC(0001) substrate with a periodicity of $2\sqrt{3} \times 2\sqrt{3} R30^\circ$. Energy values are referred to the smallest ones of the set and are plotted versus average distance between the carbon layers of graphene (right inset) and diamond-like (left inset) films. **b**, Diamond-like films with surfaces exposing chair (top two images) and boat (bottom two images) conformations, obtained by compacting two graphene layers with (from top to bottom) AB, AA, AB and A_3C stacking configurations. The top three images show films with both surfaces passivated by H. The image at the bottom of this panel has H atoms passivating only one of the two equivalent surfaces. **c**, Electronic band structure of the bottom model in **b**, with valence and conduction bands shown in red and blue, respectively. **d**, Force versus indentation curves obtained using a classical scheme based on atomistic model structures and Hookean force fields. Circles show calculated data, and solid lines show fits using a Hertz law. Simulations were carried out for a bare substrate (SiC, black) and for the same substrate coated with a 2-L film with the elastic moduli of a diamond-like (2-L-D, red) or graphene (2-L-G, green) film, as well as for a substrate coated with a 5-L graphene film (5-L-G, blue). Inset: A spherical indenter (pale red) pressing on a substrate material (blue) coated with a thin film of a stiffer material (cyan).

bonds that may be passivated by H or $-\text{OH}$ species¹³. This qualitative but important insight allows us to model the process of a hard sphere indenting a hard ultrathin film on a softer substrate. To this end, and to circumvent the limitations of continuum elasticity theory, we devised a classical scheme based on atomistic model structures and Hookean force fields. This simulation scheme, which is described in detail in the Supplementary Information, was used to calculate the force versus indentation depth curves for a substrate coated by a sub-nanometre-sized film mimicking the elastic properties of either multilayer graphene or a diamond-like film and thus exhibiting a transverse elastic modulus either ten times smaller or three times larger than that of the substrate, respectively. As shown in Fig. 4d, these indentation simulations show that a SiC(0001) substrate coated by a stiff diamond-like film yields a force versus indentation depth curve steeper than that of the bare SiC substrate, whereas a 5-L graphene film or a 2-L graphene film, which does not undergo any phase change, on SiC leads to a significant softening of the transverse mechanical response. These results are in good qualitative agreement with the experimental indentation curves reported in Figs. 1 and 2, demonstrating that only an ultrastiff 2-L film, considerably stiffer than graphene, can lead to the stiffening effect, compared to bare SiC, reported in Fig. 2.

Conclusions

Sub-ångström-resolution indentation experiments, microhardness measurements and conductive AFM investigations show that, at room temperature, pressures on the order of 1–10 GPa can reversibly transform 2-L epitaxial graphene into a diamond-like ultrastiff and ultrahard phase. A SiC(0001) substrate coated with a 2-L

epitaxial graphene film not only displays a stiffness similar to that of diamond, but it also resists perforation by a diamond indenter at loads that can create plastic indents in bare SiC, one of the hardest materials known. All these properties are not observed with graphene films thicker than three to five layers, or consisting of just the single buffer layer, proving that 2-L graphene on SiC(0001) exhibits unique mechanical properties. DFT calculations show that the observed mechanical behaviour of 2-L graphene stems from its ability to undergo a structural sp^2 to sp^3 transformation. This ability is hindered in 3-L or thicker graphene films by the occurrence of unfavourable layer-stacking configurations, whereas in 2-L graphene it is favoured by the presence of a buckled buffer layer in contact with the reactive SiC(0001) substrate. DFT calculations show that diamond-like films obtained by compressing 2-L graphene may exhibit an elastic modulus as large as 1 TPa and that formation of a diamond-like structure is not precluded by the lack of chemical species to passivate and stabilize the outer film surface. Our findings identify supported 2-L graphene as an interesting candidate for pressure-activated adaptive ultrahard and ultrathin coatings and for force-controlled dissipation switches. Our study opens up new ways to investigate graphite-to-diamond phase transitions at room temperature in low-dimensional systems. Finally, this work suggests a new route to produce and pattern single-layer diamond in graphene. For example, the diamond-like phase could be stabilized by combining local pressure with temperature, passivating gases or local heating³³, and applications could range from nanoelectronics to spintronics.

Received: 19 March 2017; Accepted: 3 November 2017;
Published online: 18 December 2017

References

- Cynn, H., Klepeis, J. E., Yoo, C. S. & Young, D. A. Osmium has the lowest experimentally determined compressibility. *Phys. Rev. Lett.* **88**, 135701 (2002).
- Narayan, J., Godbole, V. P. & White, C. W. Laser method for synthesis and processing of continuous diamond films on nondiamond substrates. *Science* **252**, 416–418 (1991).
- Jaglinski, T., Kochmann, D., Stone, D. & Lakes, R. S. Composite materials with viscoelastic stiffness greater than diamond. *Science* **315**, 620–622 (2007).
- Aust, R. B. & Drickamer, H. G. Carbon: A new crystalline phase. *Science* **140**, 817–819 (1963).
- Bundy, F. et al. The pressure-temperature phase and transformation diagram for carbon; updated through 1994. *Carbon* **34**, 141–153 (1996).
- Gorini, F. et al. On the thermodynamic path enabling a room-temperature, laser-assisted graphite to nanodiamond transformation. *Sci. Rep.* **6**, 35244 (2016).
- Horbatenko, Y. et al. Synergetic interplay between pressure and surface chemistry for the conversion of sp^2 -bonded carbon layers into sp^3 -bonded carbon films. *Carbon* **106**, 158–163 (2016).
- Khaliullin, R. Z., Eshet, H., Kühne, T. D., Behler, J. & Parrinello, M. Nucleation mechanism for the direct graphite-to-diamond phase transition. *Nat. Mater.* **10**, 693–697 (2011).
- Mao, W. L. et al. Bonding changes in compressed superhard graphite. *Science* **302**, 425–427 (2003).
- Odkhuu, D., Shin, D., Ruoff, R. S. & Park, N. Conversion of multilayer graphene into continuous ultrathin sp^3 -bonded carbon films on metal surfaces. *Sci. Rep.* **3**, 3276 (2013).
- Scandolo, S., Bernasconi, M., Chiarotti, G. L., Focher, P. & Tosatti, E. Pressure-induced transformation path of graphite to diamond. *Phys. Rev. Lett.* **74**, 4015–4018 (1995).
- Xie, H., Yin, F., Yu, T., Wang, J.-T. & Liang, C. Mechanism for direct graphite-to-diamond phase transition. *Sci. Rep.* **4**, 5930 (2014).
- Barboza, A. P. et al. Room-temperature compression-induced diamondization of few-layer graphene. *Adv. Mater.* **23**, 3014–3017 (2011).
- Rajasekaran, S., Abild-Pedersen, F., Ogasawara, H., Nilsson, A. & Kaya, S. Interlayer carbon bond formation induced by hydrogen adsorption in few-layer supported graphene. *Phys. Rev. Lett.* **111**, 085503 (2013).
- Luo, Z. et al. Thickness-dependent reversible hydrogenation of graphene layers. *ACS Nano* **3**, 1781–1788 (2009).
- Martins, L. G. P. et al. Raman evidence for pressure-induced formation of diamondene. *Nat. Commun.* **8**, 96 (2017).
- Kvashnin, A. G., Chernozatonskii, L. A., Yakobson, B. I. & Sorokin, P. B. Phase diagram of quasi-two-dimensional carbon, from graphene to diamond. *Nano Lett.* **14**, 676–681 (2014).
- Chernozatonskii, L. A., Sorokin, P. B., Kvashnin, A. G. & Kvashnin, D. G. Diamond-like C_2H nanolayer, diamane: simulation of the structure and properties. *JETP Lett.* **90**, 134–138 (2009).
- Gao, Y. et al. Elastic coupling between layers in two-dimensional materials. *Nat. Mater.* **14**, 714–720 (2015).
- de Heer, W. A. et al. Large area and structured epitaxial graphene produced by confinement controlled sublimation of silicon carbide. *Proc. Natl Acad. Sci. USA* **108**, 16900–16905 (2011).
- Riedl, C., Coletti, C. & Starke, U. Structural and electronic properties of epitaxial graphene on SiC(0001): a review of growth, characterization, transfer doping and hydrogen intercalation. *J. Phys. D* **43**, 374009 (2010).
- Palaci, I. et al. Radial elasticity of multiwalled carbon nanotubes. *Phys. Rev. Lett.* **94**, 175502 (2005).
- Lucas, M., Mai, W., Yang, R., Wang, Z. L. & Riedo, E. Aspect ratio dependence of the elastic properties of ZnO nanobelts. *Nano Lett.* **7**, 1314–1317 (2007).
- Chiu, H. C., Kim, S., Klinke, C. & Riedo, E. Morphology dependence of radial elasticity in multiwalled boron nitride nanotubes. *Appl. Phys. Lett.* **101**, 103109 (2012).
- Berger, C. et al. Electronic confinement and coherence in patterned epitaxial graphene. *Science* **312**, 1191–1196 (2006).
- Kelly, B. T. *Physics of Graphite* (Springer, London, 1981).
- Kumar, S. & Parks, D. M. Strain shielding from mechanically activated covalent bond formation during nanoindentation of graphene delays the onset of failure. *Nano Lett.* **15**, 1503–1510 (2015).
- Richter, A., Ries, R., Smith, R., Henkel, M. & Wolf, B. Nanoindentation of diamond, graphite and fullerene films. *Diam. Relat. Mater.* **9**, 170–184 (2000).
- Lucas, M., Gall, K. & Riedo, E. Tip size effects on atomic force microscopy nanoindentation of a gold single crystal. *J. Appl. Phys.* **104**, 113515 (2008).
- Deng, X., Chawla, N., Chawla, K. K., Koopman, M. & Chu, J. P. Mechanical behavior of multilayered nanoscale metal–ceramic composites. *Adv. Eng. Mater.* **7**, 1099–1108 (2005).
- Kulikovsky, V. et al. Hardness and elastic modulus of amorphous and nanocrystalline SiC and Si films. *Surf. Coat. Technol.* **202**, 1738–1745 (2008).
- Kvashnin, A. G. & Sorokin, P. B. Lonsdaleite films with nanometer thickness. *J. Phys. Chem. Lett.* **5**, 541–548 (2014).
- Wei, Z. et al. Nanoscale tunable reduction of graphene oxide for graphene electronics. *Science* **328**, 1373–1376 (2010).

Acknowledgements

The authors acknowledge support from the Office of Basic Energy Sciences of the US Department of Energy (grant no. DE-SC0016204). E.T. thanks the European ERC (320796 MODPHYSFRICT). The authors acknowledge support from the CUNY High Performance Computing Center and the Extreme Science and Engineering Discovery Environment (XSEDE). The authors thank T. Wang for support with TEM measurements, C. Dean for insights on the C-AFM measurements, and M. Moseler for discussions on indentation simulations.

Author contributions

Y.G. and F.C. performed nanomechanics experiments and data analysis. T.C. carried out DFT calculations and indentation simulations. E.R. conceived and designed the experiments and analysed the data. A.B. and E.T. analysed the experimental data and delineated the modelling strategy. C.B. and W.A.d.H. synthesized the EG samples. All authors contributed to writing the manuscript.

Competing interests

The authors declare no competing financial interests.

Additional information

Supplementary information is available for this paper at <https://doi.org/10.1038/s41565-017-0023-9>.

Reprints and permissions information is available at www.nature.com/reprints.

Correspondence and requests for materials should be addressed to E.R. or A.B.

Publisher's note: Springer Nature remains neutral with regard to jurisdictional claims in published maps and institutional affiliations.

Methods

Growth and characterization of epitaxial graphene films on SiC. Epitaxial graphene films were grown on 4H-SiC on-axis wafers by the confinement-controlled sublimation method²⁰. Details are provided in Section 1 of the Supplementary Information and in refs^{20,25,34}. For Fig. 1d,f, the buffer layer and 5-L graphene were grown on the (0001)-face (Si-face) of SiC. For Fig. 1b, 10-L graphene was grown on the (000-1)-face (C-face) of 4H-SiC. In general, films with more than ten layers were grown on the C-face. All experiments reported here on the buffer layer and 2-L graphene were performed on samples grown on the (0001)-face (Si-face) of SiC. TEM (Fig. 2 and Supplementary Fig. 1), KPFM, STEM (Supplementary Fig. 2) and Raman spectroscopy measurements were performed to characterize the epitaxial graphene samples and probe the number of graphene layers. Details are provided in ref.³⁵ and in the Supplementary Information (Supplementary Figs. 1 and 2).

MoNI stiffness measurements. A detailed description of the MoNI technique is provided in the Supplementary Information, as well as in ref.²² and in the supplementary information of ref.¹⁹ Sub-ångström vertical oscillations Δz_{piezo} were applied at 1 kHz to the AFM tip via a piezoelectric stage rigidly attached to the AFM cantilever-tip system and controlled by a lock-in amplifier, while a constant normal force F_z between the tip and the supported graphene films was maintained by a feedback loop of the AFM (see Supplementary Information for more details). An important feature of MoNI is that the tip is first brought into contact with the sample and pressed until a force on the order of 10^2 nN is reached; the tip is then retracted (over ~10s) from the surface and the variation in normal force ΔF_z at each fixed normal force F_z is measured during retraction. Integration of the measured $\Delta F_z/\Delta z_{\text{piezo}}$ at different normal loads F_z allows high-resolution force (F_z) indentation curves to be acquired. MoNI experiments were performed on standard samples such as ZnO single crystals and quartz to ensure the ability of MoNI to obtain reliable quantitative results. The typical error in force determination was $\Delta F_z = 0.5$ nN, which translates into an error in the indentation position of about $\Delta z = 0.003$ nm, for the cantilever spring constant used in our study, $k_{\text{lev}} = 173$ N m⁻¹. The estimated overall accuracy of the MoNI method was $\Delta z = 0.01$ nm. The MoNI experiments were repeated with the same AFM tip, back and forth from the SiC sample to the different graphene samples, to ensure that the tip remained unchanged. About 60 complete MoNI measurements were acquired, at different times, locations and for different samples, and showed consistent results. More details are provided in the Supplementary Information and Supplementary Figs. 4 and 5. Different methods (see Supplementary Information and Supplementary Fig. 3) were used to determine the tip radius and cantilever spring constant (typical values of ~100 nm and 173 N m⁻¹).

Microhardness measurements. The microhardness experiments presented in Fig. 3 were performed with an AFM sapphire cantilever with a diamond indenter attached (Micro Star TD10780; spring constant 151 N m⁻¹ and estimated tip radius 100 ± 50 nm). In a typical experiment, the sample was initially scanned with a set point force of 0.5–1.5 μ N to record the initial topography and remove eventual organic residues from the surface³⁶. The indentation force was applied at the centre of the scanned region by directly approaching the surface with a set point force of 12 μ N and an approaching speed of ~5 μ m s⁻¹. After indentation, the surface was scanned again with a lower set point force (<0.5 μ N) to assess the presence of the residual indent. Following ref.²⁸, the hardness H was derived according to $H = F/A$, where F is the maximum force applied with the indenter and A is the area of the residual indent determined by analysis of the AFM topography image and using different equations as described in refs^{26,29}. For more experiments with maximal loads up to 30 μ N see Supplementary Fig. 6.

C-AFM measurements. C-AFM was performed on 2-L and 5-L graphene films with AFM probes purchased from Bruker (model SCM-PTSI). The tip is made

of doped Si with a Pt coating on the apex to enhance its conductivity. The spring constant of the cantilever is 2.8 N m⁻¹. Electric current flows between the tip and a silver-paste electrode deposited close to the edge of the sample (~300 μ m). At each normal force (from 0 nN to 350 nN), a 50 nm \times 50 nm current AFM image was taken using a constant d.c. voltage of 3 mV. The average current and standard deviation error were then obtained from the current AFM images. For more details see Supplementary Information and Supplementary Fig. 7.

Computational methods. DFT calculations were carried out with tools in the QUANTUM-Espresso package^{37,38}. We used norm-conserving pseudopotentials for all atomic species, a conventional parametrization for the generalized gradient approximation of the exchange and correlation energy³⁹, a plane-wave energy cutoff larger than 80 Ry and a semi-empirical corrective scheme to account for London dispersion interactions⁴⁰. Details about the supercells, model structures, DFT optimization calculations and the method used to calculate the Young's modulus of both a diamond-like film and its interface with SiC are provided in the Supplementary Information.

Indentation simulations relied on the use of atomistic model structures and Hookean force fields. We used cubic lattices with a lattice constant of 2 Å to describe both the substrate and two-dimensional film. The substrate and two-dimensional film are periodic in the x - y plane and finite in the perpendicular (z) direction. In the x - y plane, the substrate and two-dimensional films include 40×40 cubic lattice sites, whereas in the perpendicular direction they include 15 layers for the substrate and two or five atomic layers to mimic two-dimensional films with the elastic properties of 2-L or 5-L graphene, or a stiffer diamond-like film. The first (bottom) layer of the substrate was held fixed during indentation simulations. Each lattice site is connected to its first, second and third nearest-neighbour sites via a harmonic spring with stiffness k . Sites in the same x - y plane are connected through springs with constant k_{xy} , whereas sites belonging to different layers are connected by springs with constant k_z . Values of these spring constants were calibrated to reproduce a Young's modulus of ~0.45 TPa for an isotropic substrate, a modulus of 1.2 TPa for an isotropic stiff material, and moduli parallel and perpendicular to the x - y planes of ~50 GPa and 1.2 TPa, respectively, for an anisotropic material used to mimic multilayer graphene films. Additional details are provided in the Supplementary Information.

To describe a spherical indenter and its interaction with the lattice sites of the substrate/two-dimensional film, we used a spherical Fermi–Dirac-type potential energy function, with parameters such as to mimic a tip with a radius of 5 nm and an elastic modulus close to that of diamond. Further details about the molecular-dynamics-based simulation scheme and the indentation curves shown in Fig. 4d are discussed in the Supplementary Information and Supplementary Fig. 15.

References

- Berger, C. et al. in *Graphene Growth on Semiconductors* (eds N. Motta, F. Jacopi, & C. Coletti) 181–199 (Pan Stanford Publishing Pte, Singapore, 2016).
- Filleter, T., Emtsev, K., Seyller, T. & Bennewitz, R. Local work function measurements of epitaxial graphene. *Appl. Phys. Lett.* **93**, 133117 (2008).
- Gallagher, P. et al. Switchable friction enabled by nanoscale self-assembly on graphene. *Nat. Commun.* **7**, 10745 (2016).
- Giannozzi, P. et al. QUANTUM ESPRESSO: a modular and open-source software project for quantum simulations of materials. *J. Phys. Condens. Matter* **21**, 395502 (2009).
- Kim, S. et al. Room-temperature metastability of multilayer graphene oxide films. *Nat. Mater.* **11**, 544–549 (2012).
- Perdew, J. P., Burke, K. & Ernzerhof, M. Generalized gradient approximation made simple. *Phys. Rev. Lett.* **77**, 3865 (1996).
- Grimme, S. Semiempirical GGA-type density functional constructed with a long-range dispersion correction. *J. Comput. Chem* **27**, 1787–1799 (2006).